Signature of Anomalous Exciton Localization in the Optical Response of Self-Assembled Organic Nanotubes

E. A. Bloemsma, S. M. Vlaming, V. A. Malyshev, and J. Knoester*
Zernike Institute for Advanced Materials, University of Groningen, Nijenborgh 4, 9747 AG Groningen, The Netherlands
(Received 30 May 2014; revised manuscript received 30 November 2014; published 17 April 2015)

We show that the disorder scaling of the low-temperature optical absorption linewidth of tubular molecular assemblies sharply contrasts with that known for one-dimensional aggregates. The difference can be explained by an anomalous localization of excitons, which arises from the combination of long-range intermolecular interactions and the tube's higher-dimensional geometry. As a result, the exciton density of states near the band bottom drops to zero, leading to a strong suppression of exciton localization. Our results explain the strong linear dichroism and weak exciton-exciton scattering in tubular J aggregates observed in experiments and suggest that for nanoscale wirelike applications a tubular shape is to be preferred over a truly one-dimensional chain.

DOI: 10.1103/PhysRevLett.114.156804 PACS numbers: 73.20.Mf, 71.35.Cc, 73.20.Fz, 78.67.Ch

Introduction.—In the quest for nanoscale functional materials, low-dimensional supramolecular systems that form through self-assembly from individual molecules in solution hold great potential [1–3]. Like in bulk molecular crystals, the molecules in such systems are not covalently bonded, but kept together by weaker interactions, such as van der Waals forces or hydrogen bonding. This makes self-assembled nanostructures susceptible to structural disorder, which leads to disorder in the system's microscopic parameters, such as the site energies and the intermolecular energy- and charge-transfer rates, which in turn may hinder the functional properties. For instance, a one-dimensional molecular chain easily loses its effectiveness as an energy transport wire because of disorder-induced localization of the energy-carrying states.

In this Letter, we show how self-assembled tubular molecular aggregates provide an interesting class of systems that combine the notion of a wire with the capability to counteract the strong localization effects of truly one-dimensional chains. We focus on the optical properties of tubular aggregates formed by dye molecules; these properties result from Frenkel excitons, i.e., charge neutral collective excitations. Recently tubular aggregates have raised considerable interest. Much studied examples occur in nature as light-harvesting antennas (chlorosomes) in the photosynthetic system of green sulphur bacteria [4–8]. Furthermore, various classes of synthetic dye molecules self-assemble into tubular aggregates with interesting optical properties [9–24]. All these aggregates have radii of $\sim$10 nm and lengths up to μm's.

The effects of energy and interaction disorder on the exciton states in linear molecular chains have been studied in great detail [25–31], leading to a solid understanding of their optical and energy transport properties. While much less is known about localization in tubular aggregates [32,33], experiments suggest that the exciton states in those systems are much more robust against disorder than in linear chains. First, in many tubular aggregates, a clear distinction can be made between absorption bands polarized (predominantly) parallel and perpendicular, respectively, to the tube's axis [6,9,13,16]. For perfectly ordered (cylindrically symmetric) tubes, this follows directly from optical selection rules [34]; apparently, these rules are hard to break in practice, or in other words, even in the presence of disorder, the exciton states still tend to wrap around the cylinder [33]. Second, double-quantum two-dimensional electronic spectroscopy performed on tubular aggregates of cyanine aggregates has revealed weak exciton-exciton scattering, which was interpreted as a sign of strongly delocalized exciton states [18]. Finally, low-temperature exciton-exciton annihilation was reported to be surprisingly efficient in tubular aggregates, which again suggests strongly delocalized exciton states [9].

The above experimental observations may all be explained from considering a generic microscopic exciton model for the tubular aggregate with dipolar intermolecular resonance interactions and uncorrelated site (diagonal) disorder. We show that this model predicts anomalous exciton localization. We approach the problem via the width of the absorption spectrum, which, due to the effect of exchange narrowing [26,29], is known to strongly depend on the exciton localization size. Thermal line broadening, induced by exciton-vibration scattering is neglected; if the latter gets strong enough to induce an exciton coherence size smaller than the disorder-induced localization size, disorder effects become less important and all disorder scaling relations will level off [35].

Model and numerical results.—Our model of a tubular aggregate consists of a two-dimensional sheet of molecules that is wrapped seamlessly around a cylindrical surface. This structural model has been used successfully to explain the optical spectra of the photosynthetic chlorosomes of green

bacteria and the self-assembled nanotubes of several types of synthetic dyes [11,13,15,34]. It can be shown that the aggregate in this model may be considered a stack of N_1 equidistant rings of radius R, each ring containing N_2 uniformly spaced molecules and with adjacent rings rotated relatively to each other by a helical angle γ [see inset of Fig. 1(a)] [34]. Furthermore, the molecular transition dipoles follow the cylindrical symmetry and are specified by angles α and β. Here, α is the angle between the projection of the dipole vector on the ring plane and the local tangent of the ring, and β gives the angle between the dipole vector and the cylinder axis [34]. Each molecule is identified by its position vector $\mathbf{n} = (n_1, n_2)$, with n_1 indicating the ring on which it resides and n_2 labeling the position in the ring.

The optical excitations of the aggregate are described by a Frenkel exciton model that accounts for molecular excitation energies $E_\mathbf{n}$ with uncorrelated Gaussian disorder (mean ω_0 and standard deviation σ) and nonfluctuating intermolecular transfer interactions $J_\mathbf{nm}$ determined by extended transition dipoles. The corresponding Hamiltonian reads

$$H = \sum_\mathbf{n} E_\mathbf{n} |\mathbf{n}\rangle\langle\mathbf{n}| + \sum_{\mathbf{n}\neq\mathbf{m}} J_\mathbf{nm} |\mathbf{n}\rangle\langle\mathbf{m}|, \quad (1)$$

where $|\mathbf{n}\rangle$ denotes the state in which molecule $\mathbf{n}$ is excited while all others are in the ground state.

We simulate the linear absorption spectrum, given by $A(E) = \langle \sum_q O_q \delta(E - E_q)\rangle$. Here q labels the exciton eigenstates, O_q is the oscillator strength (i.e., transition dipole squared) of state q averaged over all cylinder orientations, E_q gives the energy of state q, and $\langle\ldots\rangle$ denotes the average over disorder realizations [32]. The eigenstates, their energies, and oscillator strengths are obtained by numerical diagonalization of Eq. (1) for 10^3 disorder realizations and using the procedure of Ref. [36] to minimize numerical noise in the spectra. In all calculations, we considered cylinders of $N = 6000$ molecules.

In Fig. 1(a), we present the simulated absorption and linear dichroism spectra for parameters obtained in the analysis of experiments on tubular cyanine aggregates [13]. Thus, the two-dimensional sheet to be wrapped onto the cylinder has an oblique Bravais lattice with lattice vectors of lengths 2.0 and 0.64 nm, making an angle of $\phi = 38.7°$. The molecular transition dipoles lie along the long lattice vector and have a value of 11.4 Debye and a charge separation distance of 0.7 nm. This yields $\alpha = 0°$, the other geometric parameters depend on the radius of the cylinder and the angle Θ between the vector over which the sheet is rolled onto the cylinder and the long unit cell vector of the Bravais lattice. In the spectrum of Fig. 1(a) a radius $R = 5.455$ nm is used and a rolling angle of $\Theta = (\pi/2) - \beta = 42.6°$ [13], leading to a parameter set summarized in Table I as structure I. The disorder used in Fig. 1(a) has a magnitude of $\sigma = 600$ cm^{-1}, close to the value used to explain the experimental spectra [13].

The absorption spectrum in Fig. 1(a) clearly reveals two bands that are redshifted compared to the monomer spectrum (in this figure, we set $\omega_0 = 0$), characteristic for J aggregates. The broadening of the line shapes is induced by the energetic disorder. As is clear from the linear dichroism in Fig. 1(a), the lowest-energy J band stems from exciton

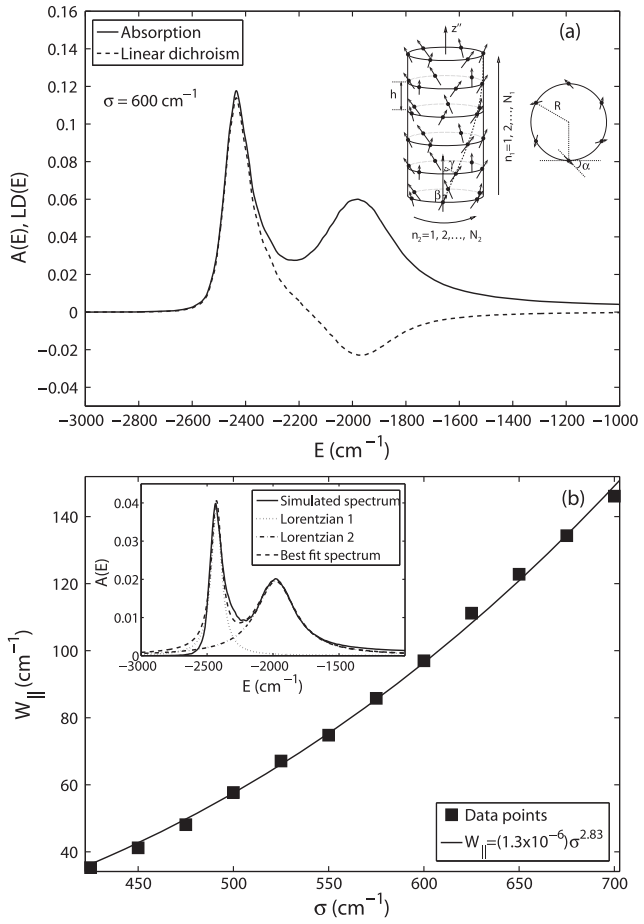

FIG. 1. (a) Isotropic absorption and linear dichroism spectra of tubular J aggregates calculated for a disorder strength $\sigma = 600$ cm^{-1} and model parameters taken from Ref. [13] (structure I, see text for details). The inset illustrates the cylindrical geometry in the stack of rings representation [34]. (b) Disorder scaling of the FWHM of the lowest absorption band. Symbols are data points, while the solid curve is the best power law fit $W_{||}(\sigma) \propto \sigma^{2.83}$. The inset shows the decomposition of the absorption spectrum into two Lorentzians.

TABLE I. Set of parameters characterizing different tubular aggregate structures: R (radius), N_2 (commensurability), β (dipole orientation), and γ (helicity). The last column represents the corresponding FWHM disorder scaling exponent B. The angle $\alpha = 0°$ in all cases. Significant changes in parameter values are indicated in bold.

Structure	R (nm)	N_2	β (degrees)	γ (degrees)	B
I	5.455	2	47.4	6.74	2.83
II	5.476	2	**−1.1**	16.7	3.29
III	**3.619**	2	45.3	10.1	3.15
IV	5.410	2	43.1	**93.4**	2.83
V	5.428	**53**	51.6	3.0	2.84

transitions polarized mainly along the tube axis, while the other band is mainly polarized perpendicular to this axis. The occurrence of two bands and their polarization properties are consistent with the optical selection rules for ordered aggregates; there, the rotational symmetry around the cylinder axis imposes a Bloch form [$\exp(2\pi i k_2 n_2/N_2)$] for the exciton wave function in the azimuthal (n_2) direction and only exciton bands with wave numbers $k_2 = 0$ (polarized parallel to the cylinder axis) and $k_2 = \pm 1$ (perpendicularly polarized) contain states that can carry oscillator strength [34].

Next, we establish the disorder scaling of the optical linewidth for aggregates of structure I. We focus on the lowest-energy absorption band, because its position at the lower exciton band edge makes its shape less sensitive to finite size effects than the high-energy one. To obtain the linewidth $W_{||}$, we first decompose the spectrum into the sum of two Lorentzian line shapes to filter the contribution of the high-energy absorption band to the width of the low-energy peak [see inset of Fig. 1(b)]. The width $W_{||}$ of the low-energy peak is taken as the full width at half maximum (FWHM) of the corresponding Lorentzian. Figure 1(b) displays the results for disorder values in the interval of $\sigma = 425$–$700\ \mathrm{cm}^{-1}$ (symbols), together with the best power law fit $W_{||}(\sigma) \propto \sigma^B$ (solid line). The disorder interval considered is bound from below due to finite size effects and from above because of overlap between the two absorption bands; we believe, however, that the power law fit accurately describes the width to considerably higher disorder values [37]. $W_{||}(\sigma)$ increases more than linearly with σ, because the number of dye molecules that coherently share an excitation decreases if σ becomes larger, thereby reducing the effect of exchange narrowing. The resulting power law exponent $B = 2.83$ differs markedly from that for one-dimensional molecular aggregates, where $B = 4/3$ for nearest-neighbor interactions and only slightly higher for long-range dipolar coupling [25,27,30].

Besides structure I, we also calculated the disorder scaling of $W_{||}$ for four other tubular structures, all based on the same molecular sheet. For each geometry, one of the model parameters R (radius), N_2 (commensurability), γ (helicity), or β (dipole orientation) was varied drastically (Table I), while the other parameters were kept close to those of structure I (within the requirements imposed by the fact that rolling the molecular sheet should lead to a seamless result). The values for R, N_2, γ, and β in the different structures are listed in Table I. The numerically obtained power-law exponents (also given in Table I) are similar for all structures considered, namely, $B \approx 3$.

Discussion.—To gain insight into the numerically obtained (large) value of the scaling exponent B, we apply the coherent potential approximation (CPA), which provides a powerful method to calculate the optical properties of disordered systems [27,32]. We closely follow the procedure outlined in Ref. [27] for one-dimensional systems. The absorption spectrum is given by

$$A(E) = \frac{1}{\pi} \frac{\Im[V(E)]}{(E - \Re[V(E)])^2 + (\Im[V(E)])^2}, \tag{2}$$

where $\Re[V(E)]$ and $\Im[V(E)]$ are the real and imaginary parts of the coherent potential $V(E)$, representing the disorder-induced shift and the half-width of the absorption spectrum, respectively. They are found as the solutions of a self-consistent equation which, in the weak disorder limit, reads

$$V(E) = \sigma^2 G[E - V(E)]. \tag{3}$$

Here, $G(E) = N^{-1} \sum_{\mathbf{k}} [E - E_{\mathbf{k}} + i0^+]^{-1}$ is the disorder-free exciton Green's function. The energies $E_{\mathbf{k}}$ are obtained from diagonalizing Eq. (1) for $\sigma = 0$.

To solve Eq. (3), the Green's function is decomposed in its real and imaginary parts, $G(E) = \Re[G(E)] + i\Im[G(E)]$. For weak disorder, $\Re[G(E)]$ is a smooth function in the vicinity of the exciton band bottom and can be approximated well by a negative constant [38]. On the other hand, $\Im[G(E)]$ equals the disorder-free density of states (DOS), defined as $D(E) = N^{-1} \sum_{\mathbf{k}} \delta(E - E_{\mathbf{k}})$.

In Fig. 2, we show the calculated DOS of the tubular aggregate of structure I in a histogram with bin size $140\ \mathrm{cm}^{-1}$ over the entire exciton band, as well as its behavior near the lower exciton band edge, E_0 (inset). The inset also displays the best power-law fit $D(E) \propto (E - E_0)^{\kappa}$ (solid curve). This reveals that the DOS drops to zero near the band bottom, approximately in a square-root-fashion, $\kappa = 0.5$. This low density of states near the band edge leads to weak disorder-induced scattering of excitons in this region; this even holds for moderate disorder (see below).

From the above, it follows that the Green's function to a good approximation can be expressed as $G(E) = -C + iD(E - E_0)^{1/2}$, where $C > 0$ and $D > 0$ are real constants. Substituting this expression into Eq. (3), we

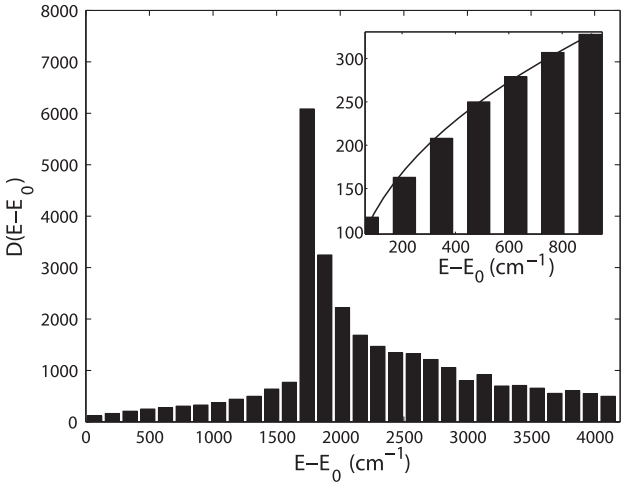

FIG. 2. Histogram (bin size $140\ \mathrm{cm}^{-1}$) of the numerically calculated DOS $D(E)$ in the absence of disorder for the tubular aggregate with parameters identical to those used in Fig. 1 (structure I). The inset shows the DOS near the lower band edge and its best power law fit (solid line) $D(E) \propto (E - E_0)^{0.44 \pm 0.06}$.

obtain the coherent potential $V(E)$ near the exciton band bottom, which, to lowest order in σ, reads

$$V(E) = -C\sigma^2 + iC^{1/2}D\sigma^3. \quad (4)$$

Thus, the CPA results in a σ^3 dependence of the FWHM of the exciton absorption spectrum, in agreement with the scaling numerically found above, $W_{||} \propto \sigma^{2.83}$. We found that also for the other structures in Table I, the scaling of $D(E)$ near the band bottom is similar ($\kappa \approx 0.5$), consistent with the above observation that the scaling powers of the FWHM all are close to $B = 3$.

The fact that the scalings for the different structures considered are similar is a consequence of the fact that all structures derive from the same molecular sheet. Indeed, for radii large compared to a single unit cell, one intuitively expects the lattice sums of dipole-dipole interactions, underlying the exciton dispersion relations on the cylinder, not to differ much from those on a flat sheet and not to depend on the radius and rolling direction anymore. It is hard to show this analytically, due to the complicated and long-range nature of these interactions. Of course, for shrinking radius, the deviations from two-dimensional behavior will grow and for very small radii one recovers the scaling relation of a one-dimensional chain. This transition cannot be described in a continuous way, due to the restrictions on rolling a two-dimensional lattice onto a cylinder in a seamless way.

Exciton localization.—The physical origin of the high value of the power B for the cylinder lies in a suppression of exciton localization near the exciton band edge, leading to an enhanced exchange narrowing effect. This suppression is a direct consequence of the vanishing DOS, which, in turn, can be traced back to an anomalous, subquadratic exciton dispersion, arising from the combination of lattice structure and long-range interactions. Indeed, for a simple two-dimensional square lattice with nearest-neighbor coupling only, one obtains $B = 2$ [25], in agreement with $D(E) =$ const near the band edge (quadratic dispersion, $\kappa = 0$).

The anomalously large exciton localization for the systems considered here can be demonstrated directly by calculating the exciton participation numbers, defined as $\mathrm{PN}_q = [\sum_{\mathbf{n}} |\nu_q(\mathbf{n})|^4]^{-1}$, where $\nu_q(\mathbf{n})$ is the exciton wave function in the site representation. The PN reflects the spatial spread of the state. Figure 3 shows the disorder scaling of the PN (for structure I) averaged over all exciton states occurring below the bare exciton band bottom. We stress, first, that the PN has an appreciable value (order of 10^3 molecules) even for a moderate disorder magnitude up to $\sigma \approx 400$ cm^{-1}. Second, the disorder scaling of the PN is linear in σ within the interval $0 < \sigma \leq 400$ cm^{-1}; this is a clear signature for the perturbative nature of the disorder. This linear scaling persists up to surprisingly large values of σ, justifying the weak-disorder limit considered when applying the CPA.

The spatial structure of the wave functions is illustrated in the inset of Fig. 3, which shows the excitation density on each molecule of the tubular aggregate for the state close to the band edge with the largest oscillator strength for one particular realization of the disorder. Compared to truly one-dimensional localized excitons, the state displayed here illustrates several interesting anomalous localization aspects. First, the exciton winds around almost the entire tube in a strongly anisotropic way: the helicity of the state follows the direction of the strongest intermolecular interactions on the cylinder. Second, there are multiple distinct regions on the tube, where the excitation density has an appreciable amplitude, reminiscent of the fractal nature of the wave functions typical for disordered two-dimensional systems [39]. Finally, the state shows long excitation tails, i.e., regions of small but nonvanishing excitation probabilities. This suggests that to a certain extent correlations between excitations in the tube can be maintained over unusually large distances, which is a favorable feature for energy transport applications.

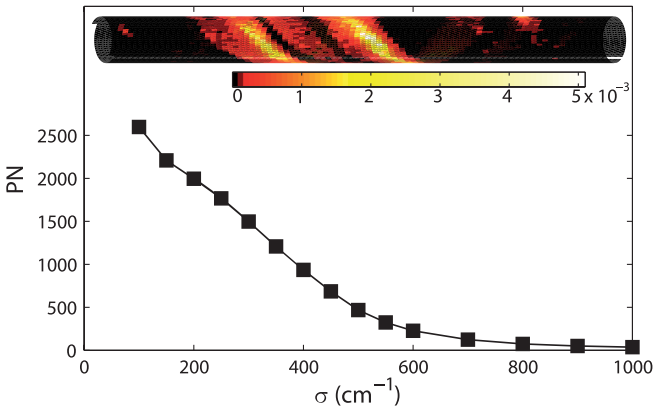

FIG. 3 (color online). Disorder scaling of the average participation number of states below the bare band bottom calculated for structure I in Table I. The inset shows the excitation density on each molecule of the aggregate for the state with largest oscillator strength for a particular disorder realization with $\sigma = 400$ cm^{-1}. The PN of the state displayed is 829; this picture is quite typical and its main features are recovered in other disorder realizations as well.

The above features are not restricted to the underlying Bravais lattice used above. We have considered a range of Bravais lattices, defined by the ratio r of the lengths of the lattice vectors and the angle ϕ between them and have found that for $0.25 \lesssim r \lesssim 0.40$ and $25° \lesssim \phi \lesssim 55°$ the DOS near the band edge vanishes, leading to suppression of localization and a scaling exponent $B > 2$. These characteristics are maintained independently of the rolling conditions, as long as the radius is large compared to a unit cell. Interestingly, the recently proposed and frequently studied structure for the chlorosomes in green sulphur bacteria [5,40,41] corresponds to $r = 0.44$ and $\phi = 36°$, on the edge of the above range. Indeed, both optical experiments and simulations have shown clear polarization properties in these systems, indicative of strong exciton delocalization [40].

Conclusions.—We have shown that excitons in self-assembled tubular molecular aggregates may be strongly

delocalized, even at the exciton band edge and for moderate values of the disorder. The weak tendency to localize derives from the fact that the DOS near the band edge vanishes, thus substantially suppressing disorder-induced exciton scattering. The vanishing DOS originates from the long-range (dipolar) intermolecular interactions in combination with the higher-dimensional structure of the aggregate. While our model calculations were restricted to uncorrelated diagonal disorder, the DOS scaling near the band edge will give rise to similar robustness against localization for other disorder models, such as off-diagonal disorder. The anomalous localization properties explain recent experiments on tubular aggregates of dye aggregates: strongly delocalized excitons may easily wrap around the cylinder (inset of Fig. 3), explaining the fact that optical spectra show strong polarization properties with respect to the tube's orientation [13,16]; strongly delocalized excitons also lead to small site occupation overlap for different exciton states, which explains the weak exciton-exciton scattering found in Ref. [18]. In addition to understanding experimental observations, we have predicted that the peculiar localization properties leave a signature in a strong disorder scaling of the absorption bandwidth. More generally, the weak tendency to localize in tubular structures may prove advantageous for their application in functional materials, such as artificial light-harvesting systems and energy transport wires.

We acknowledge D. L. Huber for fruitful discussions on the CPA.

*Corresponding author.
j.knoester@rug.nl

[1] J. M. Lehn, Proc. Natl. Acad. Sci. U.S.A. **99**, 4763 (2002).
[2] F. Würthner, T. E. Kaiser, and C. R. Saha-Möller, Angew. Chem., Int. Ed. **50**, 3376 (2011).
[3] *J-Aggregates*, edited by T. Kobayashi (World Scientific, Singapore, 2012), Vol. 2.
[4] A. R. Holzwarth and K. Schaffner, Photosynth. Res. **41**, 225 (1994).
[5] S. Ganapathy, G. T. Oostergetel, P. K. Wawrzyniak, M. Reus, A. Gomez Maqueo Chew, F. Buda, E. J. Boekema, D. A. Bryant, A. R. Holzwarth, and H. J. M. de Groot, Proc. Natl. Acad. Sci. U.S.A. **106**, 8525 (2009).
[6] Y. Tian, R. Camacho, D. Thomsson, M. Reus, A. R. Holzwarth, and I. G. Scheblykin, J. Am. Chem. Soc. **133**, 17192 (2011).
[7] M. Jendrny, T. J. Aartsma, and J. Köhler, J. Phys. Chem. Lett. **3**, 3745 (2012).
[8] G. S. Orf and R. E. Blankenship, Photosynth. Res. **116**, 315 (2013).
[9] C. Spitz, J. Knoester, A. Ouart, and S. Daehne, Chem. Phys. **275**, 271 (2002); C. Spitz and S. Daehne, Int. J. Photoenergy **2006**, 84950 (2006).
[10] S. Gandini, E. L. Gelamo, R. Itri, and M. Tabak, Biophys. J. **85**, 1259 (2003).
[11] S. M. Vlaming, R. Augulis, M. C. A. Stuart, J. Knoester, and P. H. M. van Loosdrecht, J. Phys. Chem. B **113**, 2273 (2009).
[12] A. Pawlik, S. Kirstein, U. De Rossi, and S. Daehne, J. Phys. Chem. B **101**, 5646 (1997).
[13] C. Didraga, A. Pugžlys, P. R. Hania, H. von Berlepsch, K. Duppen, and J. Knoester, J. Phys. Chem. B **108**, 14976 (2004).
[14] D. M. Eisele, J. Knoester, S. Kirstein, J. P. Rabe, and D. A. Vanden Bout, Nat. Nanotechnol. **4**, 658 (2009).
[15] D. M. Eisele, C. W. Cone, E. A. Bloemsma, S. M. Vlaming, C. G. F. van der Kwaak, R. J. Silbey, M. G. Bawendi, J. Knoester, J. P. Rabe, and D. A. Vanden Bout, Nat. Chem. **4**, 655 (2012).
[16] K. A. Clark, C. W. Cone, and D. A. Vanden Bout, J. Phys. Chem. C **117**, 26473 (2013).
[17] J. Sperling, A. Nemeth, J. Hauer, D. Abramavicius, S. Mukamel, H. F. Kauffmann, and F. Milota, J. Phys. Chem. A **114**, 8179 (2010).
[18] D. Abramavicius, A. Nemeth, F. Milota, J. Sperling, S. Mukamel, and H. F. Kauffmann, Phys. Rev. Lett. **108**, 067401 (2012).
[19] J. Yuen-Zhou *et al.*, ACS Nano **8**, 5527 2014).
[20] E. Lang, A. Sorokin, M. Drechsler, Y. V. Malyukin, and J. Köhler, Nano Lett. **5**, 2635 (2005).
[21] S. Sengupta *et al.*, Angew. Chem., Int. Ed. **51**, 6378 (2012).
[22] H. von Berlepsch and C. Böttcher, Langmuir **29**, 4948 (2013).
[23] A. V. Sorokin, I. I. Filimonova, R. S. Grynyov, G. Y. Guralchuk, S. L. Yefimova, and Y. V. Malyukin, J. Phys. Chem. C **114**, 1299 (2010).
[24] J. M. Womick, S. A. Miller, and A. M. Moran, J. Phys. Chem. A **113**, 6587 (2009); J. Phys. Chem. B **113**, 6630 (2009).
[25] M. Schreiber and Y. Toyozawa, J. Phys. Soc. Jpn. **51**, 1528 (1982); **51**, 1537 (1982).
[26] E. W. Knapp, Chem. Phys. **85**, 73 (1984).
[27] A. Boukahil and D. L. Huber, J. Lumin. **45**, 13 (1990); Phys. Lett. A **159**, 353 (1991); (private communication).
[28] F. C. Spano, Phys. Rev. Lett. **67**, 3424 (1991).
[29] A. V. Malyshev and F. Domínguez-Adame, Chem. Phys. Lett. **313**, 255 (1999).
[30] J. A. Klugkist, V. A. Malyshev, and J. Knoester, Phys. Rev. Lett. **100**, 216403 (2008).
[31] P. Walczak, A. Eisfeld, and J. S. Briggs, J. Chem. Phys. **128**, 044505 (2008); A. Eisfeld and J. S. Briggs, Phys. Rev. Lett. **96**, 113003 (2006).
[32] C. Didraga and J. Knoester, J. Chem. Phys. **121**, 10687 (2004).
[33] S. M. Vlaming, E. A. Bloemsma, M. Linggarsari Nietiadi, and J. Knoester, J. Chem. Phys. **134**, 114507 (2011).
[34] C. Didraga, J. A. Klugkist, and J. Knoester, J. Phys. Chem. B **106**, 11474 (2002).
[35] D. J. Heijs, V. A. Malyshev, and J. Knoester, Phys. Rev. Lett. **95**, 177402 (2005).
[36] D. V. Makhov, V. V. Egorov, A. A. Bagatur'yants, and M. V. Alfimov, Chem. Phys. Lett. **246**, 371 (1995).
[37] We have checked this up to $\sigma = 1200$ cm^{-1} for the arrangement in which all dipoles are oriented practically along the cylinder axis (structure II in Table I), where the higher-energy absorption band is practically absent.
[38] Negative, because it represents the second-order correction to the lowest-exciton energy.
[39] M. Schreiber, Phys. Rev. B **31**, 6146 (1985).
[40] M. Jendrny, T. J. Aartsma, and J. Köhler, Biophys. J. **106**, 1921 (2014).
[41] T. Fujita, J. Huh, S. K. Saikin, J. C. Brookes, and A. Aspuru-Guzik, Photosynth. Res. **120**, 273 (2014).